

doi.org/10.1002/minf.202100223

Pharmacophore-guided Virtual Screening to Identify New β_3 -adrenergic Receptor Agonists

Navista Sri Octa Ujiantari,^[a, b, c] Seungmin Ham,^[d] Chisae Nagiri,^[e] Wataru Shihoya,^[e] Osamu Nureki,^[e] Dana Sabine Hutchinson,^[d] and Daniela Schuster^{*(a, c)}

Abstract: The β_3 -adrenergic receptor (β_3 -AR) is found in several tissues such as adipose tissue and urinary bladder. It is a therapeutic target because it plays a role in thermogenesis, lipolysis, and bladder relaxation. Two β_3 -AR agonists are used clinically: mirabegron 1 and vibegron 2, which are indicated for overactive bladder syndrome. However, these drugs show adverse effects, including increased blood pressure in mirabegron patients. Hence, new β_3 -AR agonists are needed as starting points for drug development. Previous pharmacophore modeling studies of the β_3 -AR did not involve experimental in vitro validation. Therefore, this study aimed to conduct prospective virtual screening and confirm the biological activity of virtual hits.

Ligand-based pharmacophore modeling was performed since no 3D structure of human β_3 -AR is yet available. A dataset consisting of β_3 -AR agonists was prepared to build and validate the pharmacophore models. The best model was employed for prospective virtual screening, followed by physicochemical property filtering and a docking evaluation. To confirm the activity of the virtual hits, an in vitro assay was conducted, measuring cAMP levels at the cloned β_3 -AR. Out of 35 tested compounds, 4 compounds were active in CHO-K1 cells expressing the human β_3 -AR, and 8 compounds were active in CHO-K1 cells expressing the mouse β_3 -AR.

Keywords: β_3 -adrenergic receptors · agonist activity · pharmacophore modeling · virtual screening · GPCR

1 Introduction

The β -adrenergic receptors (β -ARs) belong to the family of G protein-coupled receptors (GPCRs).^[1] Agonists and antagonists at the β_1 -adrenergic receptor (β_1 -AR) and β_2 -adrenergic receptor (β_2 -AR) subtypes (such as salbutamol, formoterol, and propranolol) have been clinically used for decades, primarily for the treatment of asthma and cardiovascular disease.^[2] In 1989, β_3 -AR was successfully cloned and confirmed as a third subtype.^[3] Agonists at the β_3 -AR exhibited anti-obesity effects at rodent adipose tissue since it has important roles in mediating metabolic functions such as lipolysis and thermogenesis.^[4] However, β_3 -ARs were identified later in multiple tissues including urinary bladder and heart,^[5,6] where they modulate some physiological functions such as bladder relaxation, lowering or increasing cardiac contractility, and relaxation of the myometrium.^[5]

Since its discovery in the late 1980s, research has focused on identifying β_3 -AR agonists since they showed anti-obesity and anti-diabetic effects in mouse and rat models of obesity.^[7] Early β_3 -AR agonists including BRL37344 3 and CL316243 4 were potently increasing adipose tissue lipolysis, fat oxidation, insulin secretion, and insulin-mediated glucose uptake in rodents.^[7] The translation of these agonists into humans was ineffective.^[6,8] In the early 1990s, rafabegron (TAK-677) 5 was developed by Dainippon as an anti-obesity and anti-diabetic agent. However, its clinical trial failed as no significant clinical

[a] N. S. O. Ujiantari, D. Schuster
Institute of Pharmacy/Pharmaceutical Chemistry, University of Innsbruck
Innsbruck, 6020, Austria

[b] N. S. O. Ujiantari
Faculty of Pharmacy, Universitas Gadjah Mada, Yogyakarta, 55281, Indonesia

[c] N. S. O. Ujiantari, D. Schuster
Institute of Pharmacy, Department of Pharmaceutical and Medicinal Chemistry, Paracelsus Medical University
Salzburg, 5020, Austria
Phone/Fax: +43 662 2420-80610
E-mail: daniela.schuster@pmu.ac.at

[d] S. Ham, D. S. Hutchinson
Drug Discovery Biology, Monash Institute of Pharmaceutical Sciences, Monash University
Victoria, 3052, Australia

[e] C. Nagiri, W. Shihoya, O. Nureki
Department of Biological Sciences, Graduate School of Science, University of Tokyo
Tokyo 113-0033, Japan

Supporting information for this article is available on the WWW under <https://doi.org/10.1002/minf.202100223>

© 2022 The Authors. Molecular Informatics published by Wiley-VCH GmbH. This is an open access article under the terms of the Creative Commons Attribution NonCommercial License, which permits use, distribution and reproduction in any medium, provided the original work is properly cited and is not used for commercial purposes.

outcome was achieved in obese patients.^[1,9] This compound was unable to stimulate energy expenditure or fat oxidation in humans.^[10] Another compound reported by Lilly, LY377604 **6**, exerted anti-obesity effects in humans,^[1,11] however, no further studies have been published. For compound **6** as well as for several other pharmaceutical companies' compounds, poor oral bioavailability was reported as a particular problem.^[8] Compound **6** exhibited around 10–20% oral bioavailability.^[1] Most of the first series of β_3 -AR agonists contained a carboxylic acid moiety, which can undergo rapid glucuronidation during first-pass metabolism.^[1] Due to these drawbacks, the interest in the development of β_3 -AR ligands declined by 2006.^[7] Even though efforts on improving physicochemical properties to increase oral bioavailability either via a prodrug approach (e.g. esters) or via the use of acid bioisosters had been made, clinical trials still yielded disappointing data.^[1] The main cause for this poor outcome was the compound's low efficacy at the human receptor.^[8] The rodent data could not be translated into humans because of the different expression patterns of β_3 -ARs between species, particularly in adipose tissue.^[6] In humans, β_3 -AR mRNA expression is lower than in rodent adipose tissue.^[6,8] In rodents, both white and brown adipose tissues express β_3 -ARs which have roles in lipolysis and thermogenesis.^[12] However, adult humans have a predominance of white adipose tissue, which has little β_3 -AR expression. Studies showed little or no lipolysis or thermogenesis following β_3 -AR activation, which led to the lack of clinical effects of β_3 -AR agonists for the treatment of obesity and diabetes, respectively.^[12,13]

Therefore, several studies were conducted to explore other potential uses of β_3 -AR agonists.^[1] Sanofi repurposed amibegron **7** from treating metabolic disorders to treating depression as β_3 -ARs are also expressed in the brain showing antidepressant and anxiolytic activities.^[1,14] However, this drug never entered the market as the clinical trials for treatment of depression (NCT00855530) and anxiety disorder (NCT00332891) were terminated in phase III due to a lack of efficacy.^[5] Another repurposing study was conducted by GSK who had developed solabegron **8**.^[1,15] It was initially planned to be used as an antidiabetic drug but was then shifted to be used in overactive urinary bladder (OAB) syndrome.^[1] Solabegron entered phase II studies and showed promising clinical results.^[15] In contrast, the development of ritobegron **9**, another β_3 -ARs agonist for OAB treatment developed by Kissei Pharmaceuticals, was terminated in phase III (NCT01003405) because the efficacy endpoints were not met.^[1,16] Finally in 2012, the FDA approved mirabegron **1** developed by Astellas Pharma.^[1,17] It became the first clinical drug that acts via the β_3 -AR for OAB syndrome treatment under the brand name Myrbetriq.^[18] This was followed by vibegron **2**, developed by Urovant Sciences, which has been used clinically in Japan since 2018^[5,19] and was approved by the FDA in 2020 under the market name Gemtesa.^[20] Mirabegron **1** shows some adverse effects in the cardiovascular system, such as

increased blood pressure, because β_3 -ARs are also present in the myocardium and blood vessels.^[21,22] Also vibegron **2** causes adverse events such as headache, nausea, or diarrhea. Therefore, new β_3 -AR agonists are still needed as starting points for drug development.

Pharmacophore modeling is an established method in early drug discovery and development since it helps to reduce the number of compounds to be tested experimentally. The approach deploys a pharmacophore model to virtually screen compounds that fit into the model, thus predicting active compounds.^[23] Many pharmacophore modeling studies successfully yielded several promising ligands.^[24–26] Pharmacophore modeling studies using the β_3 -AR as a target were conducted previously. However, none of those studies involved experimental in vitro validation of predicted hits.^[27–31] Therefore, this study aimed to perform pharmacophore-based virtual screening and also confirm the biological activity of selected hit compounds.

2 Methods

2.1 Homology Modeling and Structure Assessment

Homology modeling was performed in SWISS-MODEL (<https://swissmodel.expasy.org/>),^[32] which relies on Pro-Mod3 v1.1.0.^[33] The human β_3 -AR (h β_3 -AR) was constructed using the user-template mode. The h β_3 -AR sequence consists of 408 amino acids and was downloaded from UniProt (<https://www.uniprot.org/>)^[34] with the primary accession number P13945. This sequence was submitted as input in SWISS-MODEL. The crystal structure of the human β_2 -AR (h β_2 -AR) (PDB-ID: 3SN6, res: 3.20 Å)^[35] was retrieved from the Protein Data Bank (www.drugbank.ca)^[36] and used as the template. Previously, the 3D structure of h β_2 -AR was analysed in Maestro v11.8.012 (Schrödinger Release 2018-4).^[37] Completion of missing loops was done using Prime (Schrödinger Release 2018-4).^[38] The ligand B1167107 bound in the crystal structure of the template was embedded into the homology model of h β_3 -AR. The homology model was prepared and minimized using the Protein Preparation Wizard (Schrödinger Release 2018-4)^[39] including protonation; creation of disulfide bonds; filling missing side chains; generate HET states with EPIK;^[40] and refinement. During the refinement, the optimization of hydrogen bonds and orientations of Asn, Gln, and His residues were assigned using PROPKA.^[41] In the end, a restrained minimization was applied using OPLS3e.^[42] Sequence alignment between h β_2 -AR and h β_3 -AR was also carried out. The quality of the final model was evaluated by the structure assessment tool in SWISS-MODEL in which runs MolProbity v4.4.^[43] In order to allow a more reliable evaluation of the model, several methods were applied:^[44]

Physics-based method. MolProbity, which is implemented in SWISS-MODEL, is used to detect backbone outliers, side-chain outliers (rotamer deviations), and inap-

appropriate all-atom contacts (atomic clashes). To detect the backbone outliers, Ramachandran outliers and C β deviation outliers are the most important ones, since both can contribute to huge errors.^[44] A Ramachandran plot is a simple bi-dimensional plot with the ϕ (phi) value on the horizontal axis and the ψ (psi) value on the vertical axis, which correspond to the protein secondary structure.^[45] This plot is divided into three regions: those where there are no interatomic clashes, those where there are moderate clashes, and those where clashes are extremely severe, considered as fully allowed, partially allowed, and forbidden, respectively.^[45] The amino acids in forbidden regions are identified as Ramachandran outliers.^[45] C β deviation outliers indicated the distortion around C α are detected in case the deviation of the observed C β atom from ideal position is >0.25 Å.^[43,46] A model is considered to have good quality when 98% of the amino acids in the Ramachandran plot are fully allowed, a maximum of 0.2% are Ramachandran outliers, and 0 for C β deviation outliers.^[43]

Knowledge-based method. In this method, Qualitative Model Energy Analysis (QMEAN), which is implemented in SWISS-MODEL, is used to calculate C β interaction energy, all-atoms pairwise energy, torsion angle energy, and solvation energy.^[44] A model with a QMEAN Z-score around 0 indicates a good agreement between the model structure and experimental structures. A QMEAN Z-score below -4 would be considered low quality.^[47]

Experiment-based method. The root-mean-square deviation (RMSD) is the simplest method which measures the distances between all the atoms in both 3D experimental and model structures.^[44] RMSD C α is used to evaluate the 3D structure model. Depending on the degree of sequence identity or similarity, and the quality of the alignment, RMSD C α can be up to $\sim 1-2$ Å,^[58] which means good accuracy.

2.2 Generation and Validation of the Pharmacophore Model

2.2.1 Dataset Preparation and Conformation Generation

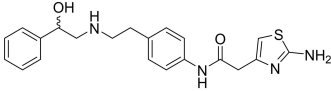
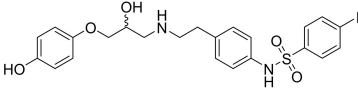
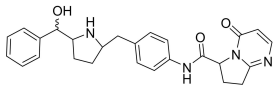
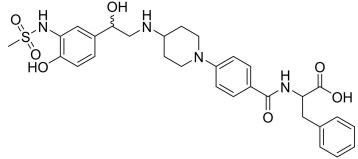
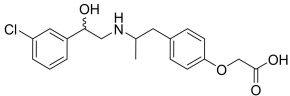
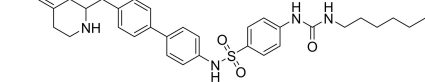
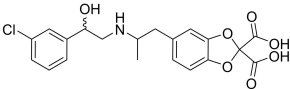
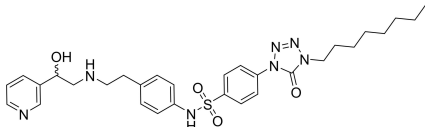
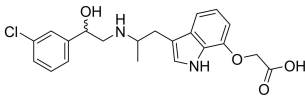
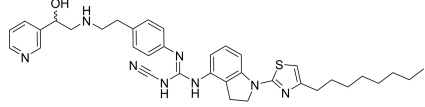
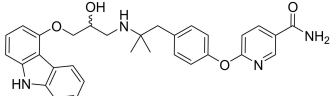
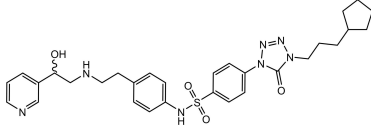
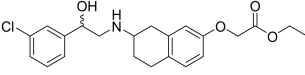
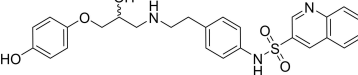
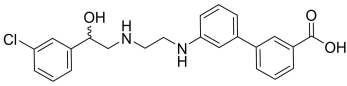
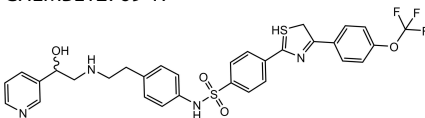
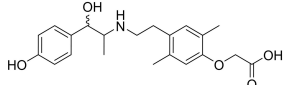
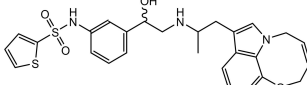
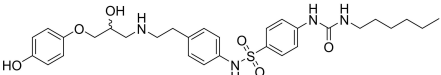
Various β_3 -AR agonists were collected from databases such as ChEMBL,^[59] PubChem,^[60] BindingDB,^[61] IUPHAR/BPS Guide to PHARMACOLOGY,^[2] and also from the literature.^[49-53,55,56,62] β_3 -AR agonists bear stereocenters or chiral centers in their structure. However, the studies related to stereochemistry of these ligands are limited. The potency of compound **3** and its isomers were investigated by Oriowo *et al.* and revealed that its RR isomer were the most potent.^[63] This finding was also supported by Harada *et al.*^[64] In addition, the RS and SR isomers exhibited similar potency and the least active, SS isomer had very low potency.^[63,64] Thus, β_3 -AR ligands activity depends on the stereochemical configuration since each isomer possesses

its own activity. However, both studies revealed that the racemic structures were potent as well. Moreover, the activity of most β_3 -AR agonists was determined based on their racemic structures. Therefore, also in the modeling part of this work, racemic structures were used. Only compounds that increased cAMP levels in cells expressing the h β_3 -AR were selected and prepared as a dataset to build and validate the pharmacophore model. Duplicates were removed by comparing the compounds' smiles codes in DataWarrior v4.7.2.^[65] The dataset contained 95 unique compounds including 11 known selective β_3 -AR agonists for which their agonist activity has been studied in preclinical or clinical studies and 84 compounds, which were classified on the basis of their activity. They were grouped according to their EC₅₀ as highly active (≤ 15 nM), moderately active (15 nM–100 nM), weakly active (100 nM–100 μ M), and inactive (EC₅₀ > 100 μ M or not determined). This dataset was split into two subsets. The training set listed in Table 1 consisted of the 11 β_3 -AR agonists investigated in (pre-)clinical studies and eight additional highly active, structurally diverse compounds. Seventy-six compounds formed the test set containing 72 active and four inactive compounds (Supporting Information Table S1). The 3D conformations of the training set compounds were generated using Omega v2.3.3^[66] with BEST settings (500 conformations/molecule) in LigandScout v3.12 (Inte:Ligand GmbH, Vienna).^[67] Because of limited inactive experimental compounds, decoys were included in the virtual screening. The SMILES codes of all the 91 active compounds from the whole dataset were used as input to generate decoys using DUD-E^[68] with standard settings (<http://dude.docking.org/>).

2.2.2 Pharmacophore Model Generation and Quality Assessment of the Pharmacophore Models

The pharmacophore models were built based on the training set. The pharmacophore features were extracted through ligand-based pharmacophore model calculations. Pharmacophore models were generated using the espresso algorithm^[23] implemented in LigandScout. In the model generation, pharmacophore fit, atom overlap and merged feature pharmacophore were selected as the scoring function and pharmacophore type, respectively. Exclusion volumes were created to represent potential steric restrictions of the binding site. In LigandScout, exclusion volume spheres are generally positioned based on an iterative placement algorithm: On a grid with 1.5 Å resolution, all points within three Å of any training set atom center with a distance of less than three Å to a hydrogen bond or a hydrophobic contact feature are considered as potential coordinates for an exclusion volume sphere. All such spheres that would clash with the van der Waals radius of any aligned training set atom are subsequently removed resulting in an exclusion volume sphere 'coat' that sterically

Table 1. Training set for the β_3 -AR pharmacophore model.

Compound structure	EC ₅₀ (nM) ^[a]	Compound structure	EC ₅₀ (nM) ^[a]
	22.4 ^[7,17]		1.6 ^[48]
Mirabegron 1		L742791 11	
	1.1 ^[19]		4 ^[49]
Vibegron 2		CHEMBL32599 12	
	21 ^[7]		6 ^[50]
BRL37344 3		CHEMBL75604 13	
	18 ^[7]		6.3 ^[51]
CL316243 4		CHEMBL22318 14	
	0.062 ^[9]		13 ^[52]
Rafabegron 5		CHEMBL127656 15	
	2.4 ^[11]		13 ^[51]
LY377604 6		CHEMBL22375 16	
	4.3 ^[7]		1.3 ^[53]
Amibegron 7		CHEMBL12769 17	
	3.98 ^[54]		4.3 ^[55]
Solabegron 8		CHEMBL331744 18	
	6.9 ^[7]		0.75 ^[56]
L755507 10		1,7-cyclized indole derivative 19	
	73 ^[16]		
	0.079 ^[57]		
	0.4 ^[7]		

^[a] The activity based on increasing cAMP level in CHO-h β_3 -AR cells.

represents the negative shape of the aligned training set molecules.

Before using the models for virtual screening, they were validated theoretically to evaluate their performance. Seventy-two active compounds, four inactive compounds,

and 6229 decoys were transformed into a screening validation database using the idbgen-tool with Omega-best settings. The assessment of the pharmacophore model quality was carried out by deploying the pharmacophore model to screen against this database. In the virtual screening process, pharmacophore fit, match all query features, and best matching conformation were selected as screening parameters for scoring function, screening mode, and retrieval mode, respectively. The parameters used for evaluating the pharmacophore model were the calculation of receiver operating characteristic (ROC) curves and enrichment factors (EFs). The ideal model depicts a steep slope ROC-curve and has a high AUC and EF value:^[69]

$$EF = \left[\frac{a}{n} \right] / \left[\frac{A}{N} \right]$$

where *a* is the number of truly active compounds retrieved by the model, *n* is the number of hits, *A* is the number of all true active compounds and *N* is the total number of compounds in the screening database.

2.3 Pharmacophore-based Virtual Screening

The selected pharmacophore model was used for virtual screening against the SPECS^[70] and Drugbank databases.^[71] These libraries containing 219,931 compounds in total were generated in LigandScout using the same settings as for the validation database. The virtual screening process followed the procedure described in section 2.2.2. Only those compounds that fitted into all features of the pharmacophore model were predicted to be active and were called hit compounds.^[23]

2.4 Selection of Hits for Biological Activity Testing

The hit compounds which fitted the pharmacophore model were considered for biological testing. However, their number was huge and additional post-screening filters were needed to select fewer hit compounds. There are two types of filters involved in this process: physicochemical properties filter and docking evaluation.

2.4.1 Physicochemical Properties Filter

The screening results were first filtered by the physicochemical parameters. The filter contained several parameters derived from β_3 -ARs agonists in the training set: molecular weight (MW 240–640); partition coefficient (ClogP 0,10–6,7); number of hydrogen acceptors ($HAC \leq 11$) and hydrogen donors ($HDO \leq 6$); polar surface area (PSA 65–180); number of rotatable bonds (RTB 3–16) and aromatic rings 2–5. These parameters were calculated in DataWarrior v4.7.2.^[65] Addi-

tionally, to ease the selection process, the screening results were also analyzed for molecular similarity using the FragFp descriptor calculated by Tanimoto metric and visualized using 2D-Ruber Band Scaling approach^[65] implemented in DataWarrior. The result of the similarity analysis was visualized as a similarity chart which displayed the chemical space of all compounds, and similar compounds are connected with a line. Based on this similarity chart, the compounds were grouped by various scaffolds.

2.4.2 Molecular Docking

The hit compounds passing the physicochemical properties filter were filtered again using a docking evaluation. The 3D structures of the compounds were prepared with Omega v2.3.3 in LigandScout. Docking was performed with GOLD v5.7.0^[72] using the docking wizard. Because no 3D structure of the human β_3 -AR was available, the homology model of h β_3 -AR described in section 2.1 was employed. ChemPLP was used as scoring function.^[73] The binding site was defined based on BI167107 as reference ligand. The cavity was set within 6 Å of the bound molecule. To evaluate the performance of the docking protocol, the validation was performed by re-docking and RMSD value calculation between the docked ligand and the reference ligand.^[74] The RMSD was 0.34 Å in this case. In general, protein-ligand docking is a tool to predict binding poses and estimate binding affinity.^[74] Therefore, docking results of hit compounds were evaluated visually to select the best interacting pose based on interactions and steric fit rather than the highest scoring pose. In summary, scaffold and/or structure variation, pharmacophore score, and docking evaluation were all considered in the selection of hit compounds for biological testing. In advance of biological activity testing, the selected compounds were examined using SciFinder (<https://scifinder.cas.org>)^[75] for known activity data including current patents to avoid double testing.

2.5 In Vitro Testing

To confirm the activity of the hit compounds, cell-based assays measuring cAMP levels were performed.

2.5.1 Materials and Assay System

The selected hit compounds were purchased from SPECS. The compounds were tested in Chinese Hamster Ovary K1 cells expressing either the human β_3 -AR (CHO-h β_3 -AR cells)^[76] or mouse β_3 -AR (CHO-m β_3 -AR cells)^[77] in order to measure the intracellular cAMP using Lance cAMP assay Kit. Clenbuterol (CLEN), BRL37344 (BRL), isoprenaline (ISO), and forskolin (FSK) were used as control compounds.

2.5.2 Measurement of cAMP Levels

Biological testing of hit compounds was described by da Silva Junior *et al.*^[78] CHO-K1 cells or CHO-K1, CHO-m β_3 -AR or CHO-h β_3 -AR cells were maintained in Dulbecco's Modified Eagle's Media: Nutrient Mixture F12 (DMEM/F12; Gibco, Cat# 10565018) containing 10% (v/v) fetal bovine serum (FBS). Media was changed twice a week and cells were incubated at 37 °C with 5% CO₂. Prior to serum-starvation (0% FBS) for 24 hours, CHO cells were plated at 1 x 10⁴/well of 96 well plates. Cells were stimulated in the final volume of 100 μ l stimulation buffer (0.1% BSA, 5 mM HEPES, HBSS, 500 μ M IBMX, pH 7.4) for 30 min at 37 °C. The stimulation was terminated by aspirating stimulation buffer and adding 50 μ l ice-cold 100% ethanol. After ethanol was evaporated, 50 μ l lysis buffer (0.1% BSA, 0.3% Tween 20, 5 mM HEPES, pH 7.4) was added to each well. The cAMP levels were quantified using 10 μ l of cell lysate or cAMP standard. After adding 5 μ l cAMP antibodies labeled with Alexa Fluor 647 in each well, 10 μ l of detection solution containing biotin-cAMP and eu-W8044 labeled streptavidin were added at room temperature in reduced light condition. Time-resolved Förster resonance energy transfer (FRET) signals were measured using a 2103 EnVision plate reader (PerkinElmer) at 340 nm excitation and 615/665 nm emission wavelengths. Concentration-response curves were analyzed by nonlinear regression between log agonist vs response three parameters to calculate pEC_{50s}.

Because β_3 -AR agonists and antagonists share similar structural features,^[8] assessment of ligands for antagonist activity was performed. Cells were treated with hit compounds (10 μ M) for 30 min before addition of the non-selective β -AR agonist isoprenaline (ISO) at a submaximal concentration (300 nM). All results are expressed as a percentage of the response to ISO. All data were calculated and analyzed using GraphPad Prism v8.2.1 (GraphPad Software, San Diego, California USA, www.graphpad.com). Statistical significance was determined using unpaired t-test with significant $P < 0.05$.

2.6 Molecular Docking of the Active Compounds into Human β_3 -AR and Mouse β_3 -AR Modelled from the Dog β_3 -AR 3D Structure

The compounds found active in the *in vitro* testing were docked into the h β_3 -AR and mouse β_3 -AR (m β_3 -AR) binding sites to evaluate their interactions in those receptors, respectively. The receptors used for docking were constructed based on the structure of the dog β_3 -AR (d β_3 -AR) (PDB ID: 7DH5, res: 3.16 Å)^[79] in Maestro v11.8.012. In addition, two h β_3 -AR models constructed from h β_2 -AR and d β_3 -AR were compared and analyzed in Maestro and SWISS-MODEL using its structure comparison tool.^[80] The parameters for the evaluation were RMSD of the respective C α atoms and the IDDT score presented as consistency value.^[80]

Molecular docking was performed as described in section 2.4.2 employing the h β_3 -AR and m β_3 -AR models, respectively. Sequence alignment among h β_3 -AR, m β_3 -AR, and d β_3 -AR was also analyzed.

3 Results and Discussion

3.1 Pharmacophore Modeling and Virtual Screening

To discover new β_3 -AR agonists, pharmacophore modeling and virtual screening were performed. Ligand-based pharmacophore modeling is suitable for this research question as there is no available 3D crystal structure of h β_3 -AR. The pharmacophore model illustrated in Figure 1A was assessed

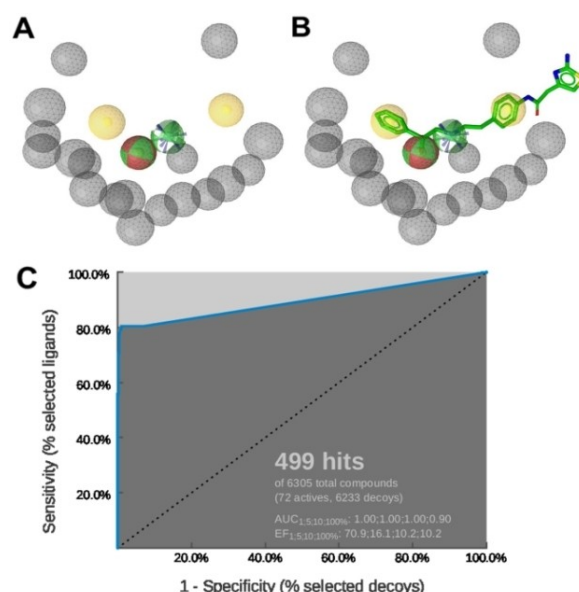


Figure 1. A: The ligand-based pharmacophore model consisted of six pharmacophore features: two hydrophobic interactions (H) – yellow; two hydrogen bond donors (HBD) – green, one hydrogen bond acceptor (HBA) – red, a positively ionizable area (PI) – blue, and 18 exclusion volumes – grey. B: Alignment of mirabegron to the pharmacophore model. C: ROC curve from the theoretical validation of the pharmacophore model. In this screening, the 499 hits found by the model contained 58 true active compounds, 1 inactive compound, and 440 decoys.

and the ROC/AUC and the EF_{100%} revealed the values 0.90 and 10.2 respectively (Figure 1C), representing the best result of the created models.

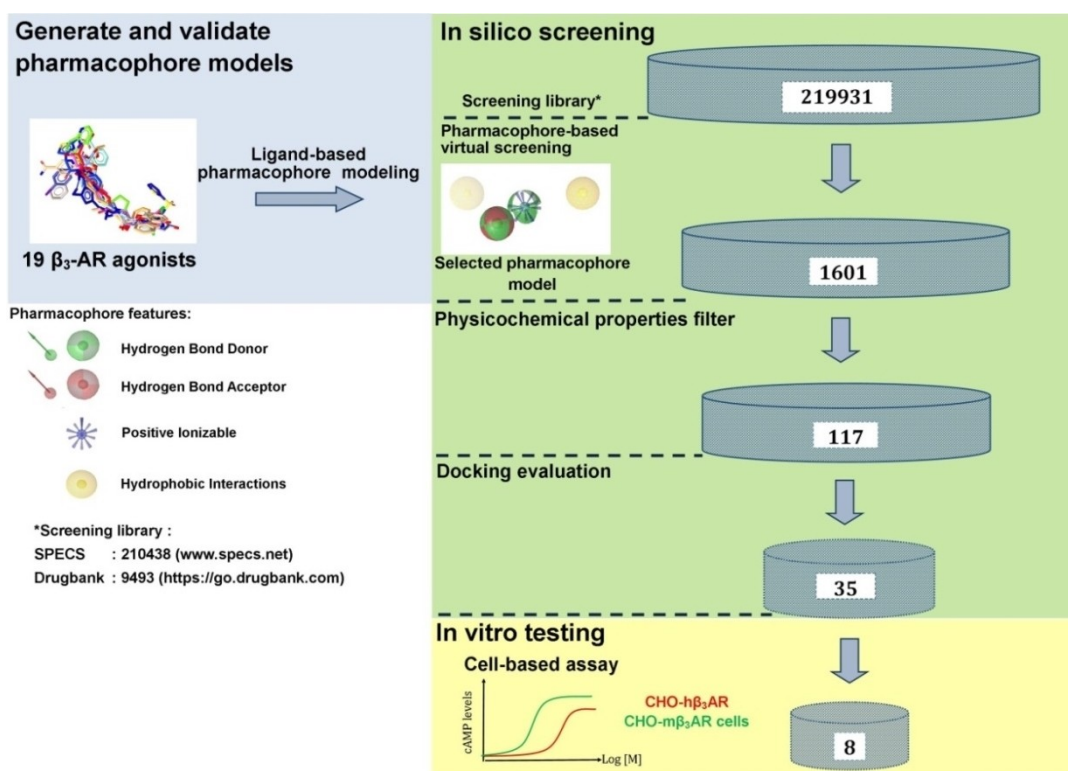
Ligand-based pharmacophore modeling for β_3 -AR ligands has previously been conducted in several studies (Table 2). However, compared to our model, they had different chemical features due to variations in the datasets and the different software tools applied to construct the models. Remarkably, some features were common in all models, namely HBD, HBA, and PI located in the center.

Table 2. Comparison of pharmacophore models.

Pharmacophore models	Size of dataset (training set, test set)	Pharmacophore features ^[a]	Software
Prathipati-Saxena model ^[27]	51 (34, 17)	RA, PI, HBD, HBA, H	Catalyst v4.6
Shakya model ^[28]	4	HBA, HBD, HBA, HpAr, HpAl, RA	Catalyst v4.7
Telvekar model ^[29]	80 (56, 24)	RA, HBA, PI, RA, RA, NI	PHASE v3.0
^[b] Jin model ^[30]	144 (35, 109)	H, PI, RA, H, HBA	Catalyst v4.10
^[b] Saxena-Roy model ^[31]	175 (51, 124)	HBD, PI, H, NI, H	Discovery Studio v2.0
Ujiantari model	95 (19, 76)	H, HBD, HBA, HBD, PI, H	LigandScout v3.12

^[a] HBD: hydrogen bond donor, HBA: hydrogen bond acceptor, PI: positive ionizable, NI: negative ionizable, H: hydrophobic interaction, RA: ring aromatic, HpAl: hydrophobic aliphatic, HpAr: hydrophobic aromatic.

^[b] The model was used in the virtual screening process, but without biological testing of hits.



Scheme 1. Workflow methodology of pharmacophore-based virtual screening for discovery new β_3 -AR agonists. The pharmacophore modeling part is shown in the blue area, the virtual screening part in the green one, and the in vitro part in the yellow one.

These features correspond to the ethanolamine moiety ($-\text{OH}-\text{C}_2\text{H}_5-\text{NH}-$), a typical scaffold of β -AR ligands.^[81] Also, most β_3 -AR agonists share similar structural features, with their ethanolamine moiety playing a central role as the minimum pharmacophore.^[1] This moiety is derived from the catecholamine structure of both the endogenous agonists adrenaline (epinephrine) and noradrenaline (norepinephrine).^[81] The hydroxyl group ($-\text{OH}$) can serve in hydrogen bonding as both HBD and HBA, whereas the amine ($-\text{NH}-$) is involved in ionic binding or as HBD. Figure 1B illustrates exactly how these features map on mirabegron. In addition, H features were found more than once, indicating that non-polar properties of ligands may

contribute to ligand-receptor interaction as well. By pharmacophore-based virtual screening (Scheme 1), 1601 compounds from two commercial screening libraries were identified as potential h β_3 -AR ligands. These compounds were filtered by physicochemical properties and similarity calculations, which yielded 117 compounds. Finally, 35 compounds were selected for biological testing. They were examined in SciFinder for potentially known agonist activities on the h β_3 -AR prior to testing (the summary of search results is provided in Supporting Information Table S2).

3.2 Homology Model of h β_3 -AR

In addition to the pharmacophore-based virtual screening, docking into a β_3 -AR homology model was conducted. Based on sequence alignment analysis, the h β_3 -AR shared 50%, 63%, and 68% by sequence identity, sequence similarity, and homology, respectively with the h β_2 -AR.

Previous homology modeling studies with the h β_3 -AR were based on the 3D structure of the h β_2 -AR.^[82,83] These models were based, however, on h β_2 -AR bound to the inverse agonist carazolol (PDB ID: 2RH1)^[84] which is an inactive conformation.^[35] Hence, the structure was modeled using the h β_2 -AR coupled to G proteins (PDB ID: 3SN6, res: 3.20 Å).^[35] This structure was chosen as a template because this is the active conformation of the h β_2 -AR bound to a β_2 -AR agonist, BI167107^[35] (Figure 2A). There are some signifi-

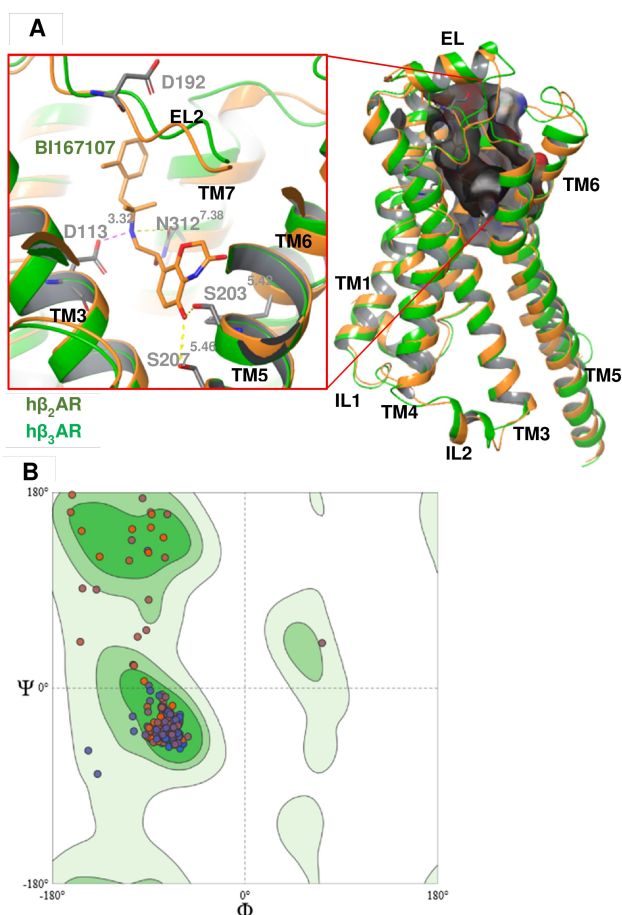


Figure 2. A: 3D Structure alignment of h β_3 -AR – green with h β_2 -AR – orange and the binding site surfaces illustrated where the ligand is oriented nearly vertical inside the binding site located in the upper part of the receptor, close to the extracellular loop 2 (EL2). In the binding site, BI167107 interacted with N312^{7,38}, D113^{3,32}, S203^{5,42}, and S207^{5,46} of h β_2 -AR through hydrogen binding. B: Ramachandran plot showing that 97.09% of amino acid residues were situated in favored regions and no Ramachandran outlier was detected.

cant differences between inactive and active structures, especially in the position of TM6. This helix differed by a 14 Å outward movement when measured at the C α of E268^{6,30}.^[35] Based on the evaluation model, results showed that 97.09% of the amino acid residues lied in favourable regions^[43] represented in Ramachandran plots (Figure 2B). RMSD C α ,^[58] C β deviations,^[43] and QMEAN Z-score^[47] were 1.2658 Å, 0, and –2.78, respectively, indicating a good quality of the model. Hence, this model was used for docking in the virtual screening process. Re-docking gave an RMSD value of 0.34 Å indicating that the docking protocol was reliable for pose prediction.

3.3 Biological Activities

In case of the β_3 -AR, binding assays are inappropriate to screen for agonist activity at the β_3 -AR due to the low affinity of the available radioligands such as [¹²⁵I]-iodocyanopindolol and [³H]-CGP 12,177.^[85] Performing functional assays including agonist-mediated increases in cAMP accumulation is a common method to test for β_3 -AR agonist activity. Thirty five compounds were tested in two types of cloned-CHO cells expressing either h β_3 -AR or m β_3 -AR. With 35 compounds tested, cAMP levels were increased by four compounds (20–23) in CHO-h β_3 -AR cells, and by 8 compounds (20–27) in CHO-m β_3 -AR cells (Figures 3–4). These increases in cAMP levels were due to actions at the β_3 -AR since none of the hit compounds or selective β -AR ligands increased cAMP levels in CHO-K1 cells lacking functional β_3 -ARs (Supporting Information Figure S1). Virtual screening yielded true positive hit rates of 11.43% and 22.86% in CHO-h β_3 -AR and CHO-m β_3 -AR cells, respectively. The agonist potency activities of active hit compounds were lower than known β_3 -AR agonists such as BRL37344 whose pEC_{50s} were 6.78 ± 0.13 and 9.16 ± 0.3 in CHO-h β_3 -AR cells and CHO-m β_3 -AR cells, respectively. In screening paradigms, a hit means a compound which has the desired activity and whose activity is confirmed upon experimental testing, typically with a potency of 100 nM–5 μ M at the target.^[86] To become preclinical candidates, further work such as hit-to-lead process and lead optimization need to be conducted. These processes mainly focus on an thorough SAR investigation around a core compound to produce more potent and selective compounds with adequate pharmacokinetic properties.^[86]

Active hit compounds contained the ethanolamine moiety verifying that this structure is the main pharmacophore to induce conformational change in the receptor instigating the cAMP signaling pathway. Interestingly, compounds 28, 29, 30, 31, and 32 (Figure 5) did not increase cAMP levels in both cell types even though they contain this moiety. These compounds lacked the phenyl group on the hydroxy end, indicating that the ring system must be present to result in agonist activity. β_3 -AR ligands had been categorized into two main chemical classes:

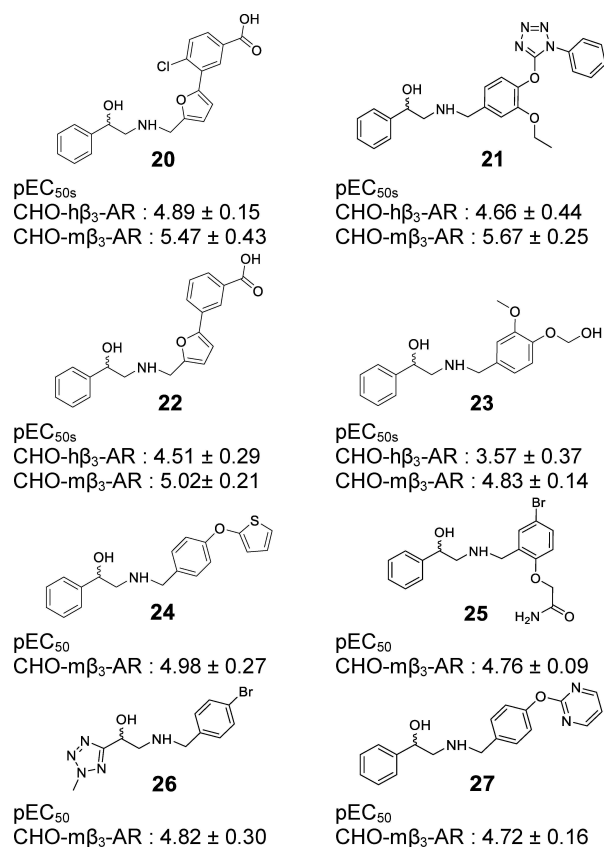


Figure 3. Hit compounds were found to be active in both cells, CHO-h β_3 -AR and CHO-m β_3 -AR cells.

arylethanolamines and aryloxypropanolamines both of which feature an aryl group on the hydroxy end.^[7,8]

In prior studies, the development of β_3 -AR agonists focused on modification of both the hydroxy and the amine end of the ethanolamine.^[1] β_3 -AR agonists were usually modified at the amine end since it was proven to improve the activity and influence receptor selectivity over the β_1 - and β_2 -AR.^[1,7] As a consequence, pharmacophore modeling studies employing ligand-based approaches extracted more hydrophobic features on the amine end (Table 2). The larger size and the presence of polar and/or ionizable functionalities seem to be beneficial to improve the activity and selectivity.^[7]

Based on the cell-based assay results, compounds **20** and **21** were the two most active ones in both the CHO-h β_3 -AR and CHO-m β_3 -AR cells. Even though compound **33** has a similar structure as compound **21**, compound **33** only increased cAMP levels in CHO-h β_3 -AR and CHO-m β_3 -AR cells by $22.00 \pm 5.23\%$ and $31.14 \pm 7.39\%$ at $100 \mu\text{M}$, respectively. Due to the presence of the ethoxy group in the phenyl ring at the amine end, compound **21**'s activity was better than compound **33**'s. In addition, the presence of a halogen substituent contributed to the higher pEC_{50} of compound **20** in comparison to compound **22**. These facts

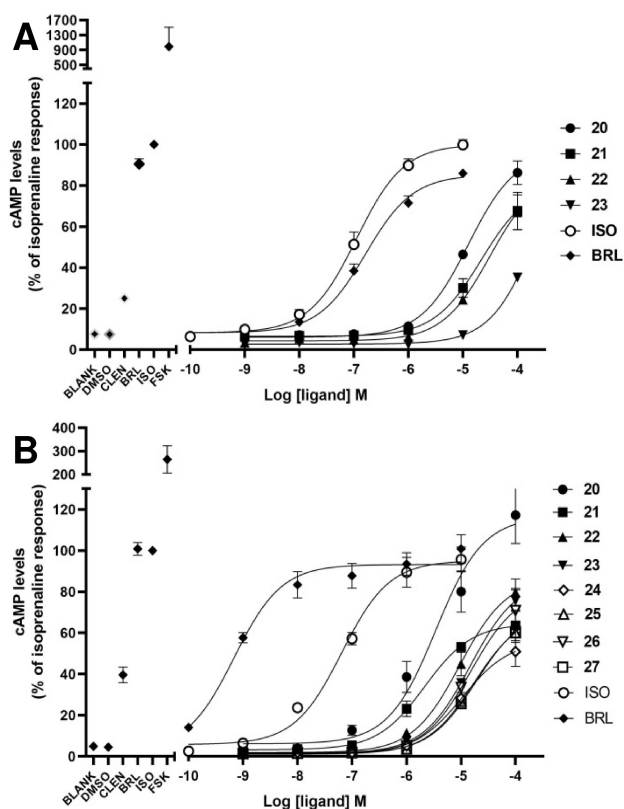


Figure 4. Concentration-dependent cAMP accumulation in CHO-h β_3 -AR cells (A) and CHO-m β_3 -AR cells (B). Eight compounds increased the cAMP level in a concentration-dependent manner in both cells whereas compound **20** exhibited maximal response in only CHO-m β_3 -AR cells at the highest concentration (B). $100 \mu\text{M}$ forskolin and $1 \mu\text{M}$ of clenbuterol (CLEN), BRL37344 (BRL) and Isoprenaline (ISO) were used as positive controls in the left of each graph. Each point represents Mean \pm SEM of 3 independent experiments performed in duplicate.

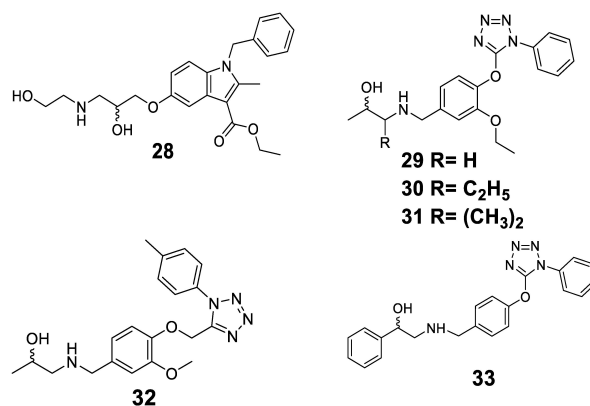


Figure 5. Hit compounds were found inactive and weakly active.

support the idea that hydrophobic moieties on the amine end would improve activity. Most β_3 -AR agonists possess an aromatic ring that is 2–3 linker atoms away from the amine

end,^[1,82] whereas our active compounds were separated by a methylene bridge. On the other hand, the phenyl or pyridyl groups are common ring systems found on the hydroxy end.^[1,7] However, compound **26** carried a smaller ring, a tetrazole group, at this position, allowing further modification on this side.

Since β_3 -AR agonists and antagonists frequently share similar molecular architecture,^[8] 35 hit compounds were tested for potential antagonistic activity (Supporting Information Figure S2). Only compound **34** (Figure 6) at

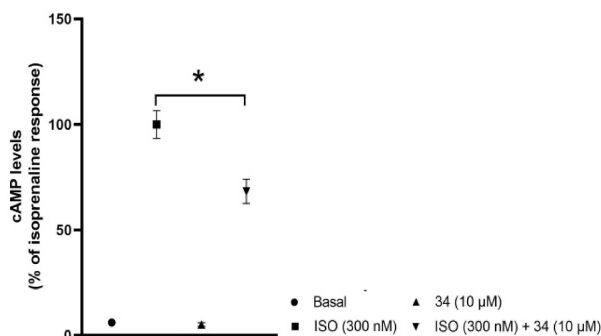


Figure 6. Hit compound was found active as a weak antagonist.

10 μ M significantly decreased the cAMP level by 31.75 % in CHO-m β_3 -AR cells when stimulated by ISO.

Hence, the pharmacophore model also identified a weak antagonist. Arch stated that the aryloxypropranolamine structure is typical of β_3 -AR antagonists.^[8] Compound **34** does not bear this structure, suggesting that the core structure of compound **34** acts as a bioisostere of the aryloxypropranolamine substructure. In the end, out of the 35 hit compounds, 26 compounds (compounds **28–33** in Figure 5 and compounds **35–54**, provided in Supporting Information Figure S3), were found to be inactive.

The eight compounds found to be active as β_3 -AR agonists in this study contained an ethanolamine moiety, and one compound with a different central moiety exhibited antagonist activity. In general, most β_3 -AR agonists contain an ethanolamine moiety at the center of structure^[1,8] because the development of β_3 -AR agonist so far rather focused on modification on the amine and hydroxyl end.^[1] This moiety was maintained or preserved since it is the main or minimum pharmacophore as it structurally represents the endogenous agonists epinephrine and norepinephrine.^[1] Our initial aim was to seek new scaffolds to replace this moiety. Nevertheless, only compounds which bear this moiety exhibited agonist activity on the β_3 -AR. However, when analyzing the novelty of a structure, the whole molecule is to be taken into account, not only a central moiety. Therefore, the discovered compounds were compared to the active compounds in the dataset using a Tanimoto metric with different fingerprints. These included hashed fingerprints and structural

keys fingerprints, which are available in Canvas^[87] (Supporting Information Section S1). Most of the newly discovered active hits had low score (< 0.5), indicating that they were structurally different from the known active compounds.

Across species, the β_3 -AR shares 80–90% homology between human, mouse, and dog.^[1,7] Recently, the 3D structure of dog β_3 -AR (d β_3 -AR) bound to mirabegron with a resolution value of 3.16 Å (PDB ID: 7DH5) was successfully determined by Cryo-EM technique.^[79] Based on the sequence alignment results, the binding sites of the human and mouse β_3 -AR differ only in three and four amino acid residues compared to the dog. Here, we assumed that there was no significant difference in the overall 3D conformation as well as the binding site and thus h β_3 -AR and m β_3 -AR were modeled based on the structure of the d β_3 -AR. Furthermore, the two h β_3 -AR models constructed from h β_2 -AR and d β_3 -AR were also compared to each other to ensure their similarity. The RMSD C α was calculated to be 1.9 Å and most of the consistency values derived from the IDDT score of each residue fell into the range of 0.5–1, which means that both models were considered identical. The detailed results and explanations are provided in Supporting Information Figures S4 and S5. The most active compounds were docked into h β_3 -AR and m β_3 -AR models to evaluate the interactions. The visualization of docking results exhibited that compound **20** and **21** aligned in a similar orientation with mirabegron interacting with the amino acid residues in the binding site of the receptor (Figure 7).

Roy and Saxena concluded based on their docking studies that the amino acid residues involved in the binding with the β_3 -AR agonists are localized in the transmembrane (TM) helices (TM3, TM5, TM6, and TM7) and extracellular loop 2 (EL2).^[82] In concordance to prior studies,^[79,82,83] the two amino acid residues D117^{3,32} and N332^{7,39} were predicted to be directly involved in binding the active compounds. At the h β_3 -AR, the hydroxyl and amine groups of the ethanolamine moiety interacted with the carboxylic acid group of D117^{3,32} and the amide group of N332^{7,39} through HBA and HBD. Besides hydrogen binding, ionic interactions were observed also between the amine group of the ethanolamine and the carboxylate ion of D117^{3,32}. A site-directed mutagenesis study conducted by Gros *et al.* proved that mutation of D117^{3,32} with leucine in h β_3 -AR led to the suppression of ligand binding and signal transduction.^[88] In addition, mutation of N332^{7,39} with alanine in d β_3 -AR reduced the potency of mirabegron 80-fold.^[79] Therefore, both residues were found to be important for ligand binding at the β_3 -AR. In addition, the phenyl ring on the hydroxy end in both compounds **20** and **21** contributed to a hydrophobic interaction with F309^{6,52}. These similar interactions were present in the docking solutions in the mouse receptor as well. Sahi *et al.* found that S208^{5,42} and Ser212^{5,46} form hydrogen bonds with the hydroxyl group of catechol of the endogenous agonists.^[83] However, most β_3 -AR agonists lack a catechol group,

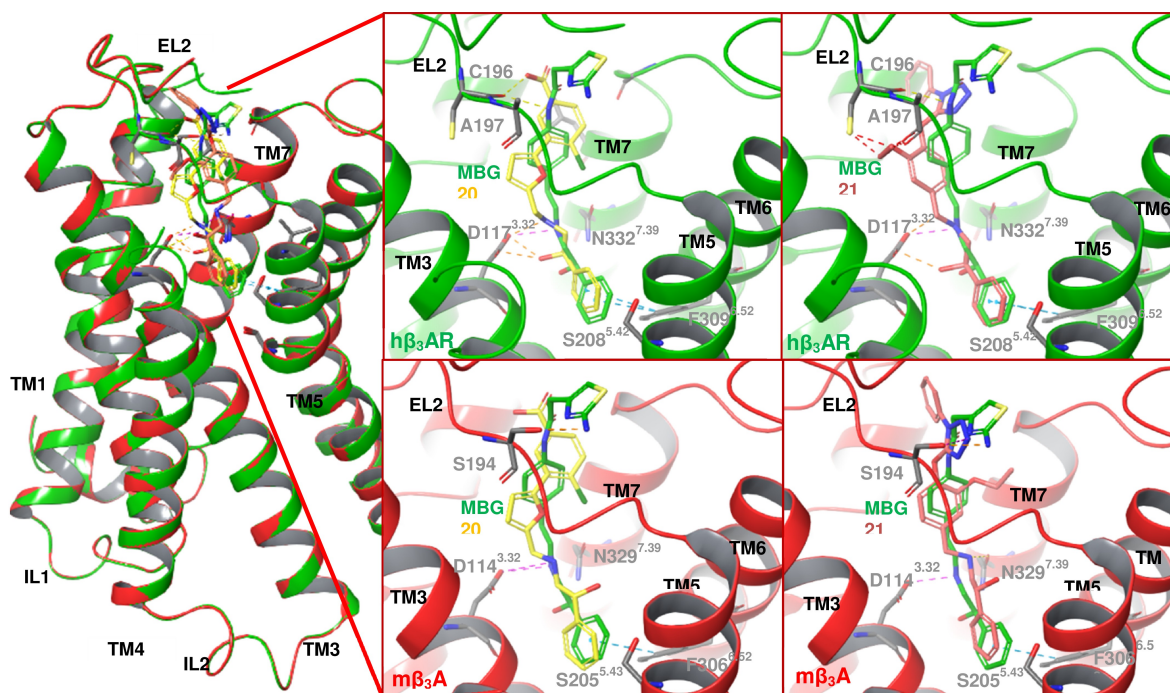


Figure 7. The interaction of **20** – yellow, **21** – pink, and mirabegron-green in $h\beta_3$ -AR and $m\beta_3$ -AR.

therefore these hydrogen bonds were mostly absent.^[82] Nagiri *et al.* proved that they are not essential for mirabegron potency by mutating these serine residues with alanine residues.^[79]

Previous studies discovered that the binding affinity and efficacy of noradrenaline and isoprenaline were higher at the human receptors than the murine receptors.^[89–91] Conversely, other β_3 -AR agonists such as adrenaline, BRL37344, and CL316243 exhibited lower affinity and efficacy at the human receptors than the rodent receptors.^[90–92] Previous studies showed that many β_3 -AR agonists were found to have low efficacy at the human receptors.^[93] Our finding also revealed more active compounds for mouse receptors compared to human receptors. This is thought to be due to subtle differences in the binding site of the rodent receptors versus human receptors.^[21] As previously stated by Roy and Saxena, A197 in the EL2 domain of the $h\beta_3$ -AR that corresponds to the aspartic acid residue at both $h\beta_1$ -AR and $h\beta_2$ -AR, must be involved in the selectivity within $h\beta$ -ARs.^[82] In line with this, the hydroxyl group of S194 (EL2) of $m\beta_3$ -ARs interacted with compound **21** (Figure 7) and mirabegron through hydrogen bonding. This suggests that this interaction may improve activity at the mouse but not the human receptors explaining why our active compounds appear to have higher activity at the mouse. However, Nagiri *et al.* tried to prove the involvement of EL2 in selectivity. Three residues in EL2 between $d\beta_3$ -AR and $h\beta_2$ -AR were swapped, namely A197, A199, and S200 of $d\beta_3$ -AR replaced by D192, F194, T195 of $h\beta_2$ -AR, and vice versa.^[79] The results showed that

these residues did not fully explain mirabegron selectivity.^[79] Based on the 3D structures of $d\beta_3$ -AR, $h\beta_2$ -AR, and $h\beta_1$ -AR, the upper part of the binding site in $d\beta_3$ -AR is narrower, thus it shapes a perpendicular cavity which may affect mirabegron selectivity.^[79] This finding may apply between human and dog β_3 -ARs since both share more similarity than mouse β_3 -AR. Therefore, the mutagenesis study in mouse may need to be carried out to understand the selectivity within species.

4 Conclusions

A ligand-based pharmacophore model for β_3 -AR agonists was developed and experimentally validated. Our approach yielded eight novel β_3 -AR agonists that can be further characterized in vitro and may serve as starting points for the further development of β_3 -AR agonists. The active compounds were more efficient at the mouse receptors compared to the human receptors. Screening of additional libraries may find compounds that are more active and could also help to improve the quality of the pharmacophore model. The ethanolamine moiety in the center of the ligand structure seemed essential for activity. In addition, agonist activity required a phenyl group at the hydroxy end. In our finding, this could be replaced by another aromatic ring system suggesting scaffold hopping. Further studies are also needed to evaluate potential bioisostere replacements for the ethanolamine moiety. In our study,

the pharmacophore model unexpectedly also detected an antagonist.

Authors Contributions

The manuscript was written through contributions of all authors. All authors have given approval to the final version of the manuscript.

Acknowledgments

We thank the Directorate General of Higher Education (DIKTI) and Österreichische Austauschdienst-Gesellschaft (OeAD) for supporting this research. Prof. Dr. Daniela Schuster is an Ingeborg Hochmair Professor of the University of Innsbruck. We acknowledge the help of Dr. Gudrun C. Thurner, Department of Pathology, Medical University of Innsbruck, and Philipp Schuster for their assistance in the manuscript preparation. Thank you to Prof. Gerhard Wolber for the technical description of the exclusion volume placement algorithm implemented in LigandScout's ligand-based pharmacophore modeling tool espresso.

Conflict of Interest

None declared.

Data Availability Statement

All relevant data are fully disclosed in the supporting information files. If further data are required, they are available from the corresponding author upon request.

References

- [1] S. D. Edmondson, *Comprehensive Medicinal Chemistry III*, Vol. 7 (Eds: S. Chackalamannil, D. Rotella, S. E. Ward), Elsevier, Oxford **2017**, pp. 714–737.
- [2] S. P. H. Alexander, A. Christopoulos, A. P. Davenport, E. Kelly, A. Mathie, J. A. Peters, E. L. Veale, J. F. Armstrong, E. Faccenda, S. D. Harding, A. J. Pawson, J. L. Sharman, C. Southan, J. A. Davies, *Br. J. Pharmacol.* **2019**, *176*, S21–S141.
- [3] L. J. Emorine, S. Marullo, M. M. B. Sutren, G. Patey, K. Tate, C. D. Klutchko, A. D. Strosberg, *Science* **1989**, *245*, 1118–1121.
- [4] J. R. S. Arch, A. T. Ainsworth, M. A. Cawthorne, V. Piercy, M. V. Sennitt, V. E. Thody, C. Wilson, S. Wilson, *Nature* **1984**, *309*, 163–165.
- [5] G. Schena, M. J. Caplan, *Cells* **2019**, *8*, 1–24.
- [6] H. Cernecka, C. Sand, M. C. Michel, *Mol. Pharmacol.* **2014**, *86*, 479–484.
- [7] J. R. S. Arch, *Eur. J. Pharmacol.* **2002**, *440*, 99–107.
- [8] M. G. Perrone, A. Scilimati, *Expert Opin. Ther. Pat.* **2011**, *21*, 505–536.
- [9] H. Harada, Y. Hirokawa, K. Suzuki, Y. Hiyama, M. Oue, H. Kawashima, H. Kato, N. Yoshida, Y. Furutani, S. Kato, *Chem. Pharm. Bull.* **2005**, *53*, 184–198.
- [10] L. M. Redman, L. d Jonge, X. Fang, B. Gamlin, D. Recker, F. L. Greenway, S. R. Smith, E. Ravussin, *J. Clin. Endocrinol. Metab.* **2007**, *92*, 527–531.
- [11] C. D. Jesudason, J. E. Baker, R. D. Bryant, J. W. Fisher, L. S. O'Farrell, G. A. Gaich, M. M. He, S. D. Kahl, A. V. Kriauciunas, M. L. Heiman, M. A. Peters, C. J. Rito, J. H. Satterwhite, F. C. Tinsley, W. G. Trankle, A. J. Shuker, *ACS Med. Chem. Lett.* **2011**, *2*, 583–586.
- [12] B. A. Evans, J. Merlin, T. Bengtsson, D. S. Hutchinson, *Br. J. Pharmacol.* **2019**, *176*, 2416–2432.
- [13] M. C. Michel, R. A. Bond, R. J. Summers, *Br. J. Pharmacol.* **2019**, *176*, 2339–2342.
- [14] D. H. Overstreet, J. Stemmelin, G. Griebel, *Pharmacol. Biochem. Behav.* **2008**, *89*, 623–626.
- [15] E. H. Ohlstein, A. V. Keitz, M. C. Michel, *Eur. Urol.* **2012**, *62*, 834–840.
- [16] I. Maruyama, Y. Goi, S. Tatemichi, K. Maruyama, Y. Hoyano, Y. Yamazaki, H. Kusama, *Naunyn-Schmiedeberg's Arch. Pharmacol.* **2012**, *385*, 845–852.
- [17] T. Takasu, M. Ukai, S. Sato, T. Matsui, I. Nagase, T. Maruyama, M. Sasamata, K. Miyata, H. Uchida, O. Yamaguchi, *J. Pharmacol. Exp. Ther.* **2007**, *321*, 642–647.
- [18] E. Sacco, R. Bientinesi, *Ther. Adv. Urol.* **2012**, *4*, 315–324.
- [19] S. J. Keam, *Drugs* **2018**, *78*, 1835–1839.
- [20] S. Yuan, Y. Q. Luo, J. H. Zuo, H. Liu, F. Li, B. Yu, *Eur. J. Med. Chem.* **2021**, *215*, 113284.
- [21] N. Dehvari, E. D. S. Junior, T. Bengsston, D. S. Hutchinson, *Br. J. Pharmacol.* **2018**, *175*, 4072–4082.
- [22] D. Staskin, J. Frankel, S. Varano, D. Shortino, R. Jankowich, P. N. Mudd, *J. Urol.* **2021**, *205*, 1421–1429.
- [23] A. Vuorinen, D. Schuster, *Methods* **2015**, *71*, 113–34.
- [24] S. M. Noha, B. Jazzar, S. Kuehn, J. M. Rollinger, H. Stuppner, A. M. Schaible, O. Werz, G. Wolber, D. Schuster, *Bioorg. Med. Chem. Lett.* **2012**, *22*, 1202–1207.
- [25] D. Schuster, C. Laggner, T. M. Steindl, A. Paluszczak, R. W. Hartmann, T. Langer, *J. Chem. Inf. Model.* **2006**, *43*, 1301–1311.
- [26] A. Vuorinen, L. G. Nashev, A. Odermatt, J. M. Rollinger, D. Schuster, *Mol. Inf.* **2014**, *33*, 15–25.
- [27] P. Prathipati, A. K. Saxena, *J. Comput.-Aided Mol. Des.* **2005**, *19*, 93–110.
- [28] N. Shakya, K. K. Roy, A. K. Saxena, *Bioorg. Med. Chem.* **2009**, *17*, 830–47.
- [29] V. N. Telvekar, D. J. Patel, N. C. Jadhav, S. J. Mishra, *Med. Chem. Res.* **2010**, *19*, 1174–1190.
- [30] F. Jin, C. Lu, X. Sun, W. Li, G. Liu, Y. Tang, *Mol. Diversity* **2011**, *15*, 817–831.
- [31] A. K. Saxena, K. K. Roy, *SAR QSAR Environ. Res.* **2012**, *23*, 389–407.
- [32] A. Waterhouse, M. Bertoni, S. Bienert, G. Studer, G. Tauriello, R. Gummienny, F. T. Heer, T. A. P. Beer, C. Rempfer, L. Bordoli, R. Lepore, T. Schwede, *Nucleic Acids Res.* **2018**, *46*, W296–W303.
- [33] G. Studer, G. Tauriello, S. Bienert, M. Biasini, N. Johnner, T. Schwede, *PLoS Comput. Biol.* **2021**, *17*, 1–18.
- [34] E. Boutet, D. Lieberherr, M. Tognolli, M. Schneider, A. Bairoch, *Plant Bioinformatics*, vol. 406 (Eds: D. Edwards), Humana Press **2007**, pp 89–112.
- [35] S. G. F. Rasmussen, H. J. Choi, D. M. Rosenbaum, T. S. Kobilka, F. S. Thian, P. C. Edwards, M. Burghammer, V. R. P. Ratnala, R.

- Sanishvili, R. F. Fischetti, G. F. X. Schertler, W. I. Weis, B. K. Kobilka, *Nature* **2011**, *477*, 549–555.
- [36] H. M. Berman, J. Westbrook, Z. Feng, G. Gilliland, T. N. Bhat, H. Weissig, I. N. Shindyalov, P. E. Bourne, *Nucleic Acids Res.* **2000**, *28*, 235–242.
- [37] Schrödinger Release 2018–4: Maestro, Schrödinger, LLC, New York, NY. **2018**.
- [38] M. P. Jacobson, D. L. Pincus, C. S. Rapp, T. J. F. Day, B. Honig, D. E. Shaw, R. A. Friesner, *Proteins* **2004**, *55*, 351–367.
- [39] G. M. Sastry, M. Adzhigirey, T. Day, R. Annabhimoju, W. Sherman, *J. Comput.-Aided Mol. Des.* **2013**, *27*, 221–234.
- [40] J. C. Shelley, A. Cholleti, L. L. Frye, J. R. Greenwood, M. R. Timlin, M. Uchimaya, *J. Comput.-Aided Mol. Des.* **2007**, *21*, 681–691.
- [41] M. H. M. Olsson, C. R. Søndergaard, M. Rostkowski, J. H. Jensen, *J. Chem. Theory Comput.* **2011**, *7*, 525–537.
- [42] K. Roos, C. Wu, W. Damm, M. Reboul, J. M. Stevenson, C. Lu, M. K. Dahlgren, S. Mondal, W. Chen, L. Wang, R. Abel, R. A. Friesner, E. D. Harder, *J. Chem. Theory Comput.* **2019**, *15*, 1863–1874.
- [43] V. B. Chen, W. B. Arendall III, J. J. Headd, D. A. Keedy, R. M. Immormino, G. J. Kapral, L. W. Murray, J. S. Richardson, D. C. Richardson, *Acta Crystallogr. Sect. D* **2010**, *66*, 12–21.
- [44] Y. Haddad, V. Adam, Z. Heger, *PLoS Comput. Biol.* **2020**, *16*, 1–19.
- [45] O. Carugo, K. D. Carugo, *Acta Crystallogr. Sect. D* **2013**, *69*, 1333–1341.
- [46] S. C. Lovell, I. W. Davis, W. B. Arendall III, P. I. W. de Bakker, J. M. Word, M. G. Prisant, J. S. Richardson, D. C. Richardson, *Proteins* **2003**, *50*, 437–450.
- [47] P. Benkert, M. Biasini, T. Schwede, *Bioinformatics* **2011**, *27*, 343–350.
- [48] A. E. Weber, H. O. Ok, R. F. Alvaro, M. R. Candelore, M. A. Cascieri, S. L. Chiu, L. Deng, M. J. Forrest, G. J. Hom, J. E. Hutchins, J. Kao, D. E. MacLntyre, R. J. Mathvink, D. McLoughlin, R. R. Miller, R. C. Newbold, T. V. Olah, E. R. Parmee, L. Perkins, R. A. Stearns, C. D. Strader, J. Szumiloski, Y. S. Tang, L. Tota, P. P. Vicario, M. J. Wyrvatt, M. H. Fisher, *Bioorg. Med. Chem. Lett.* **1998**, *8*, 2111–2116.
- [49] B. Hu, J. Ellingboe, S. Han, E. Largis, R. Mulvey, A. Oliphant, F. Sum, J. Tillett, *J. Med. Chem.* **2001**, *44*, 1456–1466.
- [50] E. R. Parmee, L. L. Brockunier, J. He, S. B. Singh, M. R. Candelore, M. A. Cascieri, L. Deng, Y. Liu, L. Tota, M. J. Wyrvatt, M. H. Fisher, A. E. Weber, *Bioorg. Med. Chem. Lett.* **2000**, *10*, 2283–2286.
- [51] T. L. Shih, M. R. Candelore, M. A. Cascieri, S. L. Chiu, L. F. Colwell Jr, L. Deng, W. P. Feeney, M. J. Forrest, G. J. Hom, D. E. MacLntyre, R. R. Miller, R. A. Stearns, C. D. Strader, L. Tota, M. J. Wyrvatt, M. H. Fisher, A. E. Weber, *Bioorg. Med. Chem. Lett.* **1999**, *9*, 1251–1254.
- [52] L. L. Brockunier, M. R. Candelore, M. A. Cascieri, Y. Liu, L. Tota, M. J. Wyrvatt, M. H. Fisher, A. E. Weber, E. R. Parmee, *Bioorg. Med. Chem. Lett.* **2001**, *11*, 379–382.
- [53] A. E. Weber, R. J. Mathvink, L. Perkins, J. E. Hutchins, M. R. Candelore, L. Tota, C. D. Strader, M. J. Wyrvatt, M. H. Fisher, *Bioorg. Med. Chem. Lett.* **1998**, *8*, 1101–1106.
- [54] Y. Igawa, M. C. Michel, *Naunyn-Schmiedeberg's Arch. Pharmacol.* **2013**, *386*, 177–183.
- [55] R. J. Mathvink, J. S. Tolman, D. Chitty, M. R. Candelore, M. A. Cascieri, L. F. Colwell Jr, L. Deng, W. P. Feeney, M. J. Forrest, G. J. Hom, D. E. MacLntyre, R. R. Miller, R. A. Stearns, L. Tota, M. J. Wyrvatt, M. H. Fisher, A. E. Weber, *J. Med. Chem.* **2000**, *43*, 3832–3836.
- [56] K. Mizuno, M. Sawa, H. Harada, I. Taoka, H. Yamashita, M. Oue, H. Tsujiuchi, Y. Arai, S. Suzuki, Y. Furutani, S. Kato, *Bioorg. Med. Chem.* **2005**, *13*, 855–868.
- [57] J. G. Baker, *Br. J. Pharmacol.* **2010**, *160*, 1048–61.
- [58] C. N. Cavasotto, S. S. Phatak, *Drug Discovery Today* **2009**, *14*, 676–683.
- [59] M. Davies, M. Nowotka, G. Papadatos, N. Dedman, A. Gaulton, F. Atkinson, L. Bellis, J. P. Overington, *Nucleic Acids Res.* **2015**, *43*, W612–W620.
- [60] S. Kim, J. Chen, T. Cheng, A. Gindulyte, J. He, S. He, Q. Li, B. A. Shoemaker, P. A. Thiessen, B. Yu, L. Zaslavsky, J. Zhang, E. E. Bolton, *Nucleic Acids Res.* **2021**, *49*, D1388–D1395.
- [61] T. Liu, Y. Lin, X. Wen, R. N. Jorissen, M. K. Gilson, *Nucleic Acids Res.* **2007**, *35*, D198–D201.
- [62] S. Tasler, R. Baumgartner, A. Aschenbrenner, A. Ammendola, K. Wolf, T. Wieber, J. Schachtner, M. Blisse, U. Quotschalla, P. Ney, *Bioorg. Med. Chem. Lett.* **2010**, *20*, 3399–3404.
- [63] M. A. Oriowo, H. Chapman, D. M. Kirkham, M. V. Sennitt, R. R. Ruffolo Jr, M. A. Cawthorne, *J. Pharmacol. Exp. Ther.* **1996**, *277*, 22–27.
- [64] H. Harada, Y. Hirokawa, K. Suzuki, Y. Hiyama, M. Oue, H. Kawashima, N. Yoshida, Y. Furutani, S. Kato, *Bioorg. Med. Chem. Lett.* **2003**, *13*, 1301–1305.
- [65] T. Sander, J. Freyss, M. V. Korff, C. Rufener, *J. Chem. Inf. Model.* **2015**, *55*, 460–473.
- [66] P. C. D. Hawkins, A. Nicholls, *J. Chem. Inf. Model.* **2012**, *52*, 2919–2936.
- [67] G. Wolber, T. Langer, *J. Chem. Inf. Model.* **2005**, *45*, 160–169.
- [68] M. M. Mysinger, M. Carchia, J. J. Irwin, B. K. Shoichet, *J. Med. Chem.* **2012**, *55*, 6582–6594.
- [69] T. Seidel, G. Wolber, M. S. Murgueitio, *Applied Chemoinformatics*, (Eds: T. Engel, J. Gasteiger), Wiley-VCH, Weinheim **2018**, pp 259–282.
- [70] Specs, Compound management services and research compounds for the life science industry, <https://www.specs.net>, accessed 26th May 2019.
- [71] D. S. Wishart 1, C. Knox, A. C. Guo, S. Shrivastava, M. Hassanali, P. Stothard, Z. Chang, J. Woolsey, *Nucleic Acids Res.* **2006**, *34*, D668–D672.
- [72] G. Jones, P. Willett, R. C. Glen, A. R. Leach, R. Taylor, *J. Mol. Biol.* **1997**, *267*, 727–748.
- [73] O. Korb, T. Stütze, T. E. Exner, *J. Chem. Inf. Model.* **2009**, *49*, 84–96.
- [74] J. Kirchmair, P. Markt, S. Distinto, G. Wolber, T. Langer, *J. Comput.-Aided Mol. Des.* **2008**, *22*, 213–28.
- [75] SciFinder, Chemical Abstracts Service, <https://scifinder.cas.org>, accessed 10th June 2019.
- [76] M. Sato, D. S. Hutchinson, B. A. Evans, R. J. Summers, *Mol. Pharmacol.* **2008**, *74*, 1417–1428.
- [77] D. S. Hutchinson, T. Bengtsson, B. A. Evans, R. J. Summers, *Br. J. Pharmacol.* **2002**, *135*, 1903–1914.
- [78] E. D. da Silva Junior, M. Sato, J. Merlin, N. Broxton, D. S. Hutchinson, S. Ventura, B. A. Evans, R. J. Summers, *Br. J. Pharmacol.* **2017**, *174*, 2318–2333.
- [79] C. Nagiri, K. Kobayashi, A. Tomita, M. Kato, K. Kobayashi, K. Yamashita, T. Nishizawa, A. Inoue, W. Shihoya, O. Nureki, *Mol. Cell* **2021**, *81*, 3205–3215.
- [80] V. Mariani, M. Biasini, A. Barbato, T. Schwede, *Bioinformatics* **2013**, *29*, 2722–2728.
- [81] B. K. Kobilka, *Trends Pharmacol. Sci.* **2011**, *32*, 213–218.
- [82] K. K. Roy, A. K. Saxena, *J. Chem. Inf. Model.* **2011**, *51*, 1405–1422.
- [83] S. Sahi, P. Tewatia, B. K. Malik, *Curr. Comput.-Aided Drug Des.* **2012**, *8*, 283–295.

- [84] V. Cherezov, D. M. Rosenbaum, M. A. Hanson, S. G. F. Rasmussen, F. S. Thian, T. S. Kobilka, H. J. Choi, P. Kuhn, W. I. Weis, B. K. Kobilka, R. C. Stevens, *Science* **2007**, *318*, 1258–1265.
- [85] W. Vrydag, M. C. Michel, *Naunyn-Schmiedeberg's Arch. Pharmacol.* **2007**, *374*, 385–398.
- [86] J. P. Hughes, S. Rees, S. B. Kalindjian, K. L. Philpott, *Br. J. Pharmacol.* **2011**, *162*, 1239–1249.
- [87] J. Duan, S. L. Dixon, J. F. Lowrie, W. Sherman, *J. Mol. Graphics Modell.* **2010**, *29*, 157–170.
- [88] J. Gros, B. S. Manning, F. P. Rouxel, J. L. Guillaume, M. F. Drumare, A. D. Strosberg, *Eur. J. Biochem.* **1998**, *251*, 590–596.
- [89] B. D. Popp, D. S. Hutchinson, B. A. Evans, R. J. Summers, *Eur. J. Pharmacol.* **2004**, *484*, 323–331.
- [90] S. B. Liggett, *Mol. Pharmacol.* **1992**, *42*, 634–637.
- [91] C. Nahmias, N. Blin, J. M. Elalouf, M. G. Mattei, A. D. Strosberg, L. J. Emorine, *EMBO J.* **1991**, *10*, 3721–3727.
- [92] D. S. Hutchinson, E. Chernogubova, M. Sato, R. J. Summers, T. Bengtsson, *Naunyn-Schmiedeberg's Arch. Pharmacol.* **2006**, *373*, 158–68.
- [93] J. R. S. Arch, *Ther. Adv. Endocrinol. Metab.* **2011**, *2*, 59–64.

Received: August 18, 2021

Accepted: December 18, 2021

Published online on February 2, 2022